Microstructure, phase inversion and yielding in immiscible polymer blends with selectively wetting silica particles

Trystan Domenech, and Sachin S. Velankar

Citation: Journal of Rheology **61**, 363 (2017);
View online: https://doi.org/10.1122/1.4975931
View Table of Contents: http://sor.scitation.org/toc/jor/61/2
Published by the The Society of Rheology

Microstructure, phase inversion and yielding in immiscible polymer blends with selectively wetting silica particles

Trystan Domenech[a] and Sachin S. Velankar[b]

Department of Chemical Engineering, University of Pittsburgh, Pennsylvania 15261

(Received 19 June 2016; final revision received 19 January 2017; published 16 February 2017)

Abstract

We examine liquid–liquid–particle ternary blends composed of two immiscible polymers and spherical silica particles across a wide range of compositions. The particles are fully wetted by one of the liquids. Rheological behavior is investigated through continuous shear flow and small/large amplitude oscillatory shear experiments. We observe various percolating structures of the particles bound by capillary interactions, as well as particles-in-drops or drops-in-suspension microstructures. These morphological changes with composition induce significant alteration in a linear viscoelastic response and yielding of the three-phase system. Similarly to the observations in wet granular materials, both the elastic plateau modulus and the yield stress of our ternary system exhibit a maximum as the wetting phase content increases for a fixed particle concentration. We show that this phenomenon is linked to an evolution of the structure from a meniscus-bridged particle network to a selectively filled bicontinuous state and eventually to a drops-in-suspension microstructure upon phase inversion. Remarkably, the presence of particles enables the formation of bicontinuous structures over a wide region of the compositional space, while no such structures could be produced for the particle-free immiscible polymer blend. This phenomenon results from selective partitioning of the particles in the wetting phase domain, which imparts a solidlike behavior of the latter due to particle crowding. Therefore, the formation of strong physical gels plays a central role in both the structure stabilization and the route to phase inversion for such ternary systems. © *2017 The Society of Rheology*. [http://dx.doi.org/10.1122/1.4975931]

I. INTRODUCTION

Suspensions and emulsions, which are, respectively, liquid–solid particle and liquid–liquid two-phase mixtures, are major classes of soft materials. Despite their simple definition, these materials have a complex rheological behavior, which depends on the volume fraction of the dispersed phase and the interactions between their components. More specifically, these systems can behave either as liquids or as soft viscoelastic solids, e.g., due to the colloidal glass transition in the case of suspensions [1] and dense packing of the droplets for emulsions [2]. What happens when suspensions and emulsions are combined—i.e., when particles and two liquids are present—is the topic of this article.

The combination of two immiscible fluids with solid particles is ubiquitous in industrial applications. Such ternary systems implicitly share common background with suspensions and emulsions, yet they present some unique morphological properties. One well-studied example of three-phase liquid–liquid–solid particle systems is particle-stabilized emulsions, widely known as Ramsden–Pickering emulsions, where particles act as surfactants by adsorbing at the liquid–liquid interface, hence inhibiting drop coalescence [3–5]. This scenario is however favored only if the particles are partially wetted by both of the immiscible liquid phases. The same concept has been used in polymer blends, where interfacially active colloidal particles are incorporated during melt-mixing [6]. Additionally, particle-stabilized emulsions can assemble into volume-spanning networks through particle-bridging [7,8], where a coherent particle monolayer at the liquid–liquid interface locally connects the droplets via capillary adhesion [9,10]. The presence of interfacially active particles can also serve to stabilize the bicontinuous structure through arrested spinodal decomposition of the fluids as in the case of *bijels* (bicontinuous interfacially jammed emulsion gels) [11–13], with analogous cases in polymer blends [14–17].

The above examples can be regarded, at least conceptually, as the effect of adding a small amount of particles to an emulsion. Recent research endeavors have focused on the opposite situation, i.e., starting with a particulate suspension and then adding a second immiscible liquid [18–24]. In this scenario, small amounts of the emulsified wetting phase can impart a significant increase in shear modulus and yield stress of the suspension due to the formation of capillary bridges connecting the particles. Hence, the use of the capillary bridge as a physical bond in suspensions, which can be disrupted and reformed via mixing, serves as a new tuning parameter of their rheology through the formation of non-equilibrium structures. This approach, inspired by the cohesion of wet granular materials [25], has strong potential for applications as it offers a new assembly pathway for functional materials [26,27]. Moreover, even a single ternary system can display several of the above morphologies depending on its composition.

To summarize, ternary systems are capable of forming a variety of complex microstructures through diverse ways,

[a]Present address: Matière Molle et Chimie, ESPCI Paris – CNRS, UMR-7167, PSL Research University, 10 rue Vauquelin, 75005 Paris, France.
[b]Author to whom correspondence should be addressed; electronic mail: velankar@pitt.edu

e.g., pairwise attraction through capillary bridging [18,21,22], many-body cohesion through capillary clustering [22], interfacial assembly of particles [11,12], or particle bridging of drops [7,8].

Because the mechanical response of liquid–liquid–solid particle systems is highly sensitive to the ternary composition, it is of considerable interest to investigate the rheology of these systems and how it relates to their microstructure. This is of immediate relevance to melt-processing from the perspective of materials production. Due to the presence of volume-spanning network structures in ternary systems, the latter can be categorized within the broad class of materials known as *yields stress fluids*.

Previous reviews have proposed the idea of a generic microstructural map for ternary particle-fluid-liquid mixtures [26,28]. This map is well established only in restricted regions of the composition space for various experimental systems. Previous studies from our group focused on the influence of particle wettability [8] and mixing conditions [20,21] on the resulting structures of ternary systems, as well as structure–rheology relationships in Pickering gels [8] and pendular gels [22]. However, a detailed morphological map and a clear understanding of the rheology of the various microstructures are still lacking for these systems. Furthermore, the influence of selective particle-filling on phase inversion of ternary systems remains unclear.

The current study seeks to map the microstructure and rheology of ternary systems with strong preferential wetting of the particles by one of the liquid phases throughout a wide region of the compositional space. Specifically, the particle volume fraction ranges from 0 to 0.3, and the volumetric ratio of the immiscible liquids is varied from very small to large values—a composition range that has not been covered in a single experimental system. As in our recent studies, we use a model ternary blend of polyisobutylene (PIB), poly(ethylene oxide) (PEO), and silica particles (SPs). This system allows us to easily freeze the blend morphology by simple cooling of the samples following melt mixing. One of the polymer phases is then selectively extracted and the microstructure characterized via electron microscopy. Furthermore, since both polymers behave as Newtonian fluids, any non-Newtonian rheological behavior from the ternary systems can be attributed to structural effects linked to the presence of particles. Using this model system, we first consider the variations in linear viscoelasticity resulting from changes in the wetting phase content. Next, we present the role of the wetting phase content on the yielding behavior of the ternary system. To this end, we discuss large amplitude oscillatory shear (LAOS), continuous shear, and creep tests in order to uncover the elasto-viscoplastic nature of these materials. Then, we address the issue of phase inversion composition in these systems, where the glassy rheology of the filled polymer phase plays an important role. Finally, we construct a morphological map for this ternary system over a range of particle loadings from 0 to 30 vol. %. To our knowledge, this is the most detailed microstructural map for a single liquid–liquid–solid particle mixture to date.

II. EXPERIMENTS

A. Three-phase blend preparation

The materials used in this study are same as those in our previous publications [21,22,29]. The solid particles are spherical SPs supplied by Industrial Powders (SS1205). The size distribution provided by the supplier indicates a unimodal polydisperse size distribution, from which a number-average diameter of 2.0 μm and a volume-average diameter of 2.3 μm can be calculated. Two polymers were used as immiscible fluids. The nonwetting phase is PIB with $\rho = 0.908\,\mathrm{g\,ml^{-1}}$ and $\bar{M}_w = 2200\,\mathrm{g\,mol^{-1}}$, purchased from Soltex, while the wetting phase is PEO with $\rho = 1.1\,\mathrm{g\,ml^{-1}}$ and $\bar{M}_w = 20\,000\,\mathrm{g\,mol^{-1}}$, purchased from Fluka. Physically, PIB is a viscous liquid whereas PEO is a semicrystalline solid powder at room temperature, with a melting point around 60 °C. The formation of the ternary blends was achieved through a two-step melt-mixing process using a small-scale mixing device (for a detailed description of the mixing cell, see [22]). First, a PEO-in-PIB or PIB-in-PEO pre-emulsion was prepared at 1200 rpm for 2 min, followed by the addition of the SPs and subsequent mixing of the three phases at 1000 rpm for 5 min. Mixing was always carried out at 80 °C so that PEO remained in the liquid state. An amount of approximately 4 g per batch was recovered, sealed in plastic jars, and rapidly cooled to 5 °C for crystallization of PEO. After recovering to room temperature, samples were placed under vacuum to remove the entrapped air bubbles from the bulk material. The ternary composition is defined by the volume fraction of particles ϕ, the wetting phase (PEO) volume fraction ϕ_{PEO}, and the volume fraction of PIB, $\phi_{\mathrm{PIB}} = 1 - \phi - \phi_{\mathrm{PEO}}$. The samples are referred to by their PIB/PEO/SP volume fractions in % for easier reading.

B. Morphological characterization

Our ternary system allows solidifying the wetting phase by simple cooling, which facilitates electron microscopy. Observations at the particle scale were carried out using a Philips XL30 field emission gun scanning electron microscope (FEG-SEM). For samples with a high PIB content, the samples were prepared for imaging identically to our previous studies: The PIB phase was removed via selective dissolution using *n*-octane (Sigma Aldrich), and the solid residue was deposited on a filter paper for imaging. At high PEO content, the solid phase became continuous. In such cases, the entire sample was cryofractured in liquid nitrogen to ensure brittle fracture of the PEO phase. The sample was then allowed to return to room temperature in an inert atmosphere to avoid water condensation on the surface. The fractured samples were then exposed to *n*-octane to remove the PIB. In all cases, the surface of the specimens (either the solid residue on filter paper or the fracture surface) was metalized to enhance electron conductivity using a sputter coater equipped with a gold–palladium target (Cressington). The samples were placed on SEM stubs prior to observations

using a secondary electron detector under high vacuum conditions.

C. Rheological measurements

The rheological characterization was performed on a TA Instruments AR-2000 stress-controlled rotational rheometer fitted with an air convection oven. Rough boundary conditions were imposed by using a cross-hatched parallel plate geometry (diameter of 25 mm, gap of 1 mm, roughness of 500 μm). This was necessary due to the previous experimental evidence of apparent wall slip at large deformations when using smooth geometries for similar ternary systems [21]. All measurements were performed at 80 °C so that the PEO phase is in the melt state. Linear viscoelastic spectra were obtained from frequency sweeps, where the angular frequency ω was varied from 100 to 0.1 rad s^{-1} at a fixed strain amplitude γ_0. Strain sweeps tests were used to determine the linear viscoelastic domain as well as to probe the LAOS behavior, where the strain amplitude γ_0 was increased from 6×10^{-5} to 1 with $\omega = 1$ rad s^{-1}. In complement to the linearized viscoelastic moduli, the relative intensities of odd harmonics contribution to the stress waveforms were calculated using a fast Fourier transform algorithm. Yielding under a continuous flow was investigated via stress ramp tests, where σ was increased from 10 to 5000 Pa in a time interval $\Delta t = 10$ min. For these tests, the measured viscosity corresponds to a transient state and must be considered as an *apparent* viscosity, especially at low stresses where the equilibration time t_{eq} to reach steady state can be very long, i.e., $t_{eq} > \Delta t$. Finally, the transient behavior under creep was determined by imposing a constant shear stress σ while measuring the strain γ and shear rate $\dot{\gamma}$ over time.

III. RESULTS

A. Structural evolution associated with wetting phase content

To characterize the structure of ternary blends, we performed SEM observations after selective removal of the PIB phase from PIB/PEO/SP samples at a fixed particle volume fraction of $\phi = 0.30$, with a PEO volume fraction ϕ_{PEO} ranging from 0.07 to 0.63. As mentioned in the Introduction, our previous research had focused on the $0 \leq \phi_{PEO} \leq \phi$ composition range, and the scientific questions mainly revolved around two issues: The effects of meniscus formation between particles when $\phi_{PEO} \ll \phi$, and the effects of particle engulfment by PEO when $\phi_{PEO} \approx \phi$. In contrast, the composition range covered here is much broader and encompasses all intermediate cases between simple SP-in-PIB and SP-in-PEO suspensions. Figure 1 shows micrographs at magnifications selected to match the appropriate microstructural length-scale of each sample. At the lowest PEO content ($\phi_{PEO} = 0.07$), the sample exhibits an aggregated structure with particles forming a three-dimensional network [Fig. 1(a)]. The interparticular bonding of this network is ensured by small capillary bridges of PEO, as detailed in previous studies [21,22], corresponding to a *pendular* state [30]. Indeed, the ϕ_{PEO}/ϕ ratio of 0.23 in Fig. 1(a) falls in the range of 0.15–0.25 within which well-developed pendular networks were noted previously [22]. For $\phi_{PEO} = 0.14$, a similar structure is observed, yet the strands of the particle network become more compact [Fig. 1(b)]. This case corresponds to a *funicular* state [30], i.e., a pendular structure where a fraction of the capillary bridges have coalesced locally due to the increase in wetting phase content. Further increase in PEO ($\phi_{PEO} = 0.21$) marks a distinctive structure, with capillary aggregates partially merged together into a continuous network [Fig. 1(c)]. An alternative view of this structure can be seen in the lower magnification image in Figure S1 of the Supplementary Material [31]. These particle clusters typify the *capillary* state [30], where the cohesion between the solid particles arises from the negative Laplace pressure linked to the negative curvature of the fluid–fluid interface, hence resulting in an attractive capillary force. Partial coalescence of these capillary aggregates results in an arrested bicontinuous state. Similar bicontinuous structures are observed at higher PEO contents, where the characteristic domain size increases with the PEO volume fraction as shown in Fig. 1(d) ($\phi_{PEO} = 0.28$) and Fig. 1(e) ($\phi_{PEO} = 0.35$). Strikingly, the SPs tend to protrude from the PIB–PEO interface of the aggregates at lower ϕ_{PEO} [see Fig. 1(c)] while a much smoother interface is observed at higher ϕ_{PEO} [see Figs. 1(d) and 1(e)]. On a side note, the term *bicontinuous* may require clarification for these ternary systems since pendular and funicular network structures can be also considered as physically bicontinuous. However, we only refer to a structure as bicontinuous when both liquid phases present in the ternary system (i.e., PIB and PEO) form continuous paths, as for the samples shown in Figs. 1(c)–1(e).

Phase inversion is achieved for the following sample composition ($\phi_{PEO} = 0.42$), where the PEO is the only continuous polymer phase as can be observed in Fig. 1(f). The voids left by the extracted dispersed phase (i.e., PIB) reveal the presence of both spherical and nonspherical drops, all featuring a wide size distribution, while the SPs are exclusively localized in the PEO phase. Such nonspherical droplet structures may result from the formation of large PIB inclusions that could not fully relax to a spherical drop shape within the particle-filled PEO continuous phase before the sample was quenched. We have not tested whether a slower quench would allow relaxation of these drops to spherical shape. The final three compositions ($\phi_{PEO} = 0.49$, 0.56, and 0.63) lead to a similar *drops-in-suspension* structure, yet elongated drops can no longer be observed [Figs. 1(g)–1(i)]. As ϕ_{PEO} increases, the dispersed phase (PIB) volume fraction decreases, leading to a marked decrease in the PIB drop size of the drops-in-suspension [see Figs. 1(g)–1(i)]. Notably, the craters corresponding to the extracted PIB drops in Figs. 1(f)–1(i) show smooth surfaces with minimal protrusion of the particles across the PIB–PEO interface, which confirms the full wetting of the particles by the PEO phase.

B. Linear viscoelasticity

We start to examine the rheology of these ternary systems by probing their linear viscoelastic response through frequency sweep measurements. The frequency-dependence of the storage (G') and loss (G'') moduli at 80 °C in the linear domain for the ternary samples is shown in Fig. 2, where the

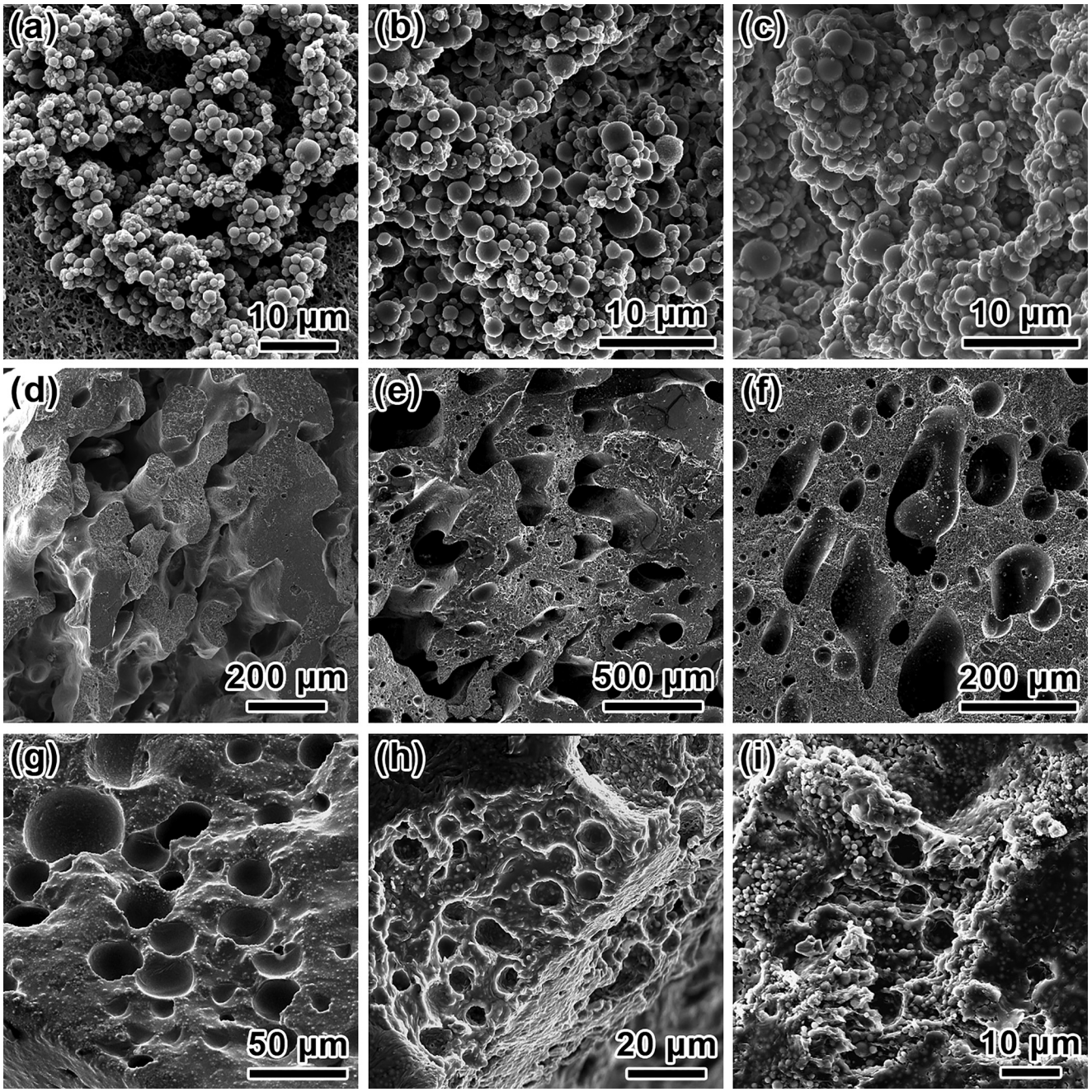

FIG. 1. SEM pictures of the PEO–SP structures after selective dissolution of the PIB phase for the following ternary systems: (a) 63/7/30, (b) 56/14/30, (c) 49/21/30, (d) 42/28/30, (e) 35/35/30, (f) 28/42/30, (g) 21/49/30, (h) 14/56/30, and (i) 7/63/30, where the ternary composition is given as PIB/PEO/SP in vol. %. The particle volume fraction is fixed at $\phi = 0.30$, while the PEO (wetting phase) volume fraction ϕ_{PEO} is gradually increased.

angular frequency ω was decreased from 10^2 to 10^{-1} rad/s. Variations in the limit of linearity with ternary samples composition will be presented in Sec. III C. In the absence of particles, PEO and PIB are almost purely viscous and we were unable to measure the very small G' values reliably. When no wetting phase is added ($\phi_{\mathrm{PEO}} = 0$), a solidlike response characterized by a weakly frequency-dependent G' plateau with $G' > G''$ over most of the investigated ω-range is found. Moreover, the presence of a local minimum in G'' is suggestive of long time (α) and short time (β) relaxation processes, a rheological signature consistently encountered in colloidal gels and glasses [1,32]. The minimum in $G''(\omega)$ occurs for $\omega = 1/\lambda_m$, where λ_m represents the crossover time from the β to the α relaxation. This solidlike behavior characterizes binary PIB/SP suspensions for $\phi \gtrsim 0.25$, where the interactions between the particles turn the suspension into an elastic paste, as shown in a previous study [22]. Similar behavior is found for ternary systems when the wetting phase volume fraction increases up to $\phi_{\mathrm{PEO}} = 0.07$. However, we notice a significant increase in elastic plateau modulus G'_p, while the G'' minimum moves toward higher frequencies and the gap between G' and G'' becomes more pronounced in this range of wetting phase content ($0 < \phi_{\mathrm{PEO}} \leq 0.07$). The inverse trend is observed for $\phi_{\mathrm{PEO}} > 0.07$, i.e., with increasing ϕ_{PEO}, the G' plateau decreases while the G'' minimum shifts to lower frequencies and G'' approaches G'. In fact, the elastic

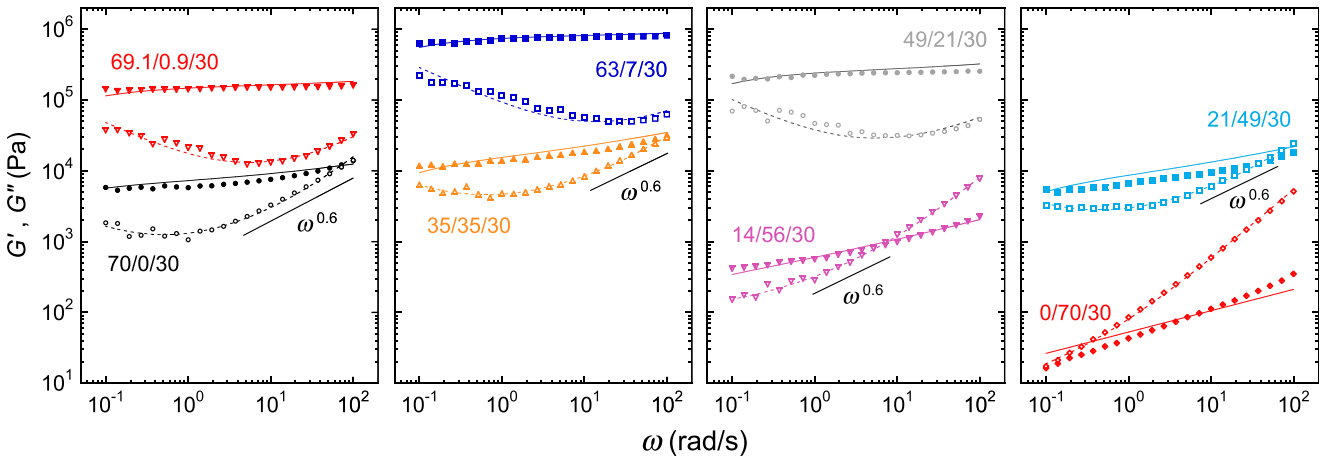

FIG. 2. Linear viscoelastic response of the ternary systems at 80 °C for $\phi = 0.30$ and $0 \leq \phi_{\mathrm{PEO}} \leq 0.7$. Filled symbols, G'; open symbols, G''. Solid and dashed lines correspond to fits using Eqs. (1) and (2), respectively. Results are split in four graphs in order to enhance clarity.

plateau modulus becomes much less pronounced for $\phi_{\mathrm{PEO}} \geq 0.49$, indicating the softening of the ternary system. The short-time moduli crossover is then observed within the experimental frequency window. In the case of the PEO/SP suspension ($\phi_{\mathrm{PEO}} = 0.70$), an overall liquidlike response ($G' < G''$) is found within the measurement window, although there appears to be a crossover around $\omega = 0.1\,\mathrm{rad\,s^{-1}}$. The contrast between the linear responses of the binary SP-in-PIB and SP-in-PEO suspensions at equal particle content is likely indicative of differences in particle attractions: Since PIB has much lower polarity than the silica, particles tend to aggregate in PIB, thus increasing G'. In contrast, PEO is much more polar, and the particles likely act as near-hard spheres. We note that as ω increases toward the high-frequency crossover, the loss modulus roughly scales as $G''(\omega) \sim \omega^{0.6}$ for these ternary systems, similar to the concentrated systems such as emulsions [33,34] and foams [35] where a power-law exponent of 0.5 is found.

Quantitatively, the linear viscoelastic spectra depicted in Fig. 2 can be well described using the model of Mason and Weitz [1], initially developed for concentrated hard sphere suspensions near the glass transition. This model is based on the formalism of mode-coupling theory (MCT) to account for the glassy cage dynamics, while the high-frequency behavior is defined through hydrodynamic contributions based on Brownian motion and suspension viscosity. Within this framework, the frequency dependence of the moduli is expressed as follows:

$$G'(\omega) = G'_p + G_\sigma\left[\Gamma(1-a')\cos\left(\frac{\pi a'}{2}\right)(\omega t_\sigma)^{a'} - B\Gamma(1+b')\cos\left(\frac{\pi b'}{2}\right)(\omega t_\sigma)^{-b'}\right] + G'_D(\omega), \quad (1)$$

$$G''(\omega) = G_\sigma\left[\Gamma(1-a')\sin\left(\frac{\pi a'}{2}\right)(\omega t_\sigma)^{a'} + B\Gamma(1+b')\sin\left(\frac{\pi b'}{2}\right)(\omega t_\sigma)^{-b'}\right] + G''_D(\omega) + \eta_\infty\omega, \quad (2)$$

where the plateau modulus G'_p only accounts for the elasticity of the structure, while the viscoelastic amplitude G_σ influences both the change of $G'(\omega)$ in the plateau region and the minimum value of $G''(\omega)$, which has reached for $\omega = 1/t_\sigma$ (thus, $t_\sigma \equiv \lambda_m$). $\Gamma(x)$ is the gamma function and the parameters $a' = 0.301$, $b' = 0.545$, and $B = 0.903$ correspond to MCT predictions for hard spheres. The viscous contribution is embodied by the high-frequency suspension viscosity η_∞. Both $G'(\omega)$ and $G''(\omega)$ include the same Brownian contribution based on the diffusional boundary layer

$$G'_D(\omega) = G''_D(\omega) = \frac{3}{5\pi}\frac{k_BT}{R^3}\phi^2 g(2R,\phi)[\omega\tau_D]^{1/2}, \quad (3)$$

where R is the particle radius, $g(2R,\phi) = 0.78/(0.64-\phi)$ is the radial pair distribution function at contact, $\tau_D = R^2/D_s$ is the diffusional time, and D_s is the short-time diffusion coefficient, which is ϕ-dependent. In the present case, the contribution of Brownian motion is weak, and therefore, the $G'_D(\omega)$ and $G''_D(\omega)$ terms can be ignored. Hence, we use Eqs. (1) and (2) to simultaneously fit $G'(\omega)$ and $G''(\omega)$ for each set of data presented in Fig. 2 with G'_p, G_σ, t_σ, and η_∞ as fitting parameters (listed in Table I), setting the $G'_D(\omega)$ and $G''_D(\omega)$ terms to zero. We emphasize that even though there are four fitting parameters, three can be pinned down almost exactly by simple inspection: G'_p corresponds to the plateau modulus, and the values of t_σ and G_σ can be calculated from

TABLE I. Fitting parameters for the linear viscoelastic data shown in Fig. 2. Sample compositions refer to PIB/PEO/SP volume %.

Sample	ϕ_{PEO}/ϕ	G'_p (Pa)	G_σ (Pa)	t_σ (s)	η_∞ (Pa s)
70/0/30	0	5.93×10^3	10^3	3.17	124
69.1/0.9/30	0.03	1.5×10^5	1.06×10^4	0.305	117
63/7/30	0.23	7.84×10^5	4.07×10^4	0.130	120
49/21/30	0.7	2.43×10^5	2.41×10^4	0.357	130
35/35/30	1.17	1.05×10^4	3.79×10^3	2.97	186
21/49/30	1.63	5×10^3	2.33×10^3	4.43	159
14/56/30	1.87	1.25×10^2	1.12×10^2	76.4	71
0/70/30	2.33	0	2.9	9315	54

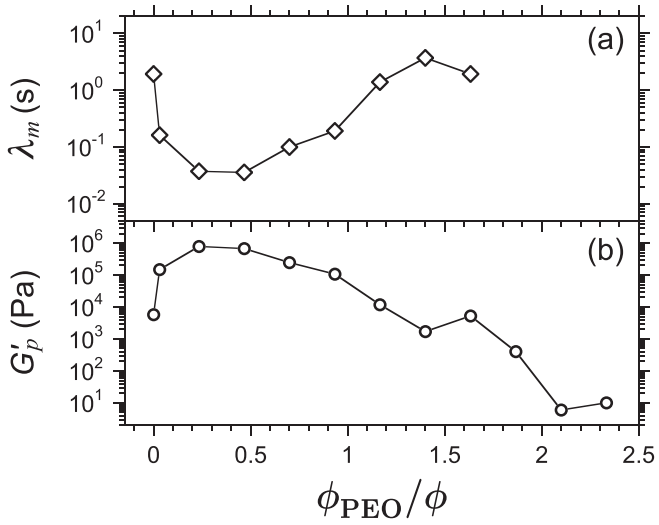

FIG. 3. (a) Characteristic time for the local minimum in $G''(\omega)$ and (b) elastic plateau modulus vs wetting phase-to-particle volume ratio for $\phi = 0.30$.

the location and magnitude of the minimum in G''. Thus, η_∞ is the only parameter that is truly free to fit the data since its value cannot be measured reliably for many of the samples (the high-frequency Newtonian regime was often out of the experimental frequency window). Importantly, the ternary systems considered here are well below the glass transition (expected at a particle volume fraction of 0.56 [36]) and therefore their solidlike properties reflect a gel state rather than a glass state, implying that MCT might not be relevant for these systems. Nevertheless, even if the model introduced by Mason and Weitz is based on MCT, its functional forms for $G'(\omega)$ and $G''(\omega)$ very well capture the glasslike viscoelasticity of these ternary systems, as shown by the solid and dashed lines in Fig. 2.

To illustrate the rheological sensitivity to the wetting phase volume fraction, we plot λ_m and G'_p as functions of ϕ_{PEO}/ϕ in Fig. 3. A striking feature here is the nonmonotonic evolution of these parameters with increasing ϕ_{PEO}, and hence with ϕ_{PEO}/ϕ (since ϕ is fixed). Most remarkably, G'_p starts to increase by two decades to reach a plateau and then exhibits a significant decrease as ϕ_{PEO}/ϕ keeps increasing. The initial rise in G'_p translates the strengthening of the elastic particle network due to a progressive interparticle bonding through the creation of capillary bridges [18,21,22]. The plateau region is reached for $0.2 \lesssim \phi_{PEO}/\phi \lesssim 0.5$, consistent with the previous findings at much lower particle volume fraction ($\phi = 0.10$) [22], where the maximum in G'_p corresponds to the transition from pendular to funicular state. On the other hand, λ_m shows the opposite trend as G'_p when ϕ_{PEO} increases (note that no G'' minimum was found for $\phi_{PEO}/\phi \gtrsim 1.7$). Such simultaneous increase in G'_p and lowering of λ_m when the materials strengthen via capillary bridging is reminiscent of the reinforcing effects linked to the increase in the particle volume fraction, as shown in our previous study on pendular gels [22] as well as in the case of colloidal depletion gels [32].

C. LAOS

We used dynamic strain sweeps to determine the nonlinear viscoelastic response of these systems. Figure 4 traces $G'(\gamma_0)$ and $G''(\gamma_0)$ for various ternary compositions, with the angular frequency fixed at $\omega = 1\,\mathrm{rad\,s^{-1}}$. For strain amplitudes exceeding the linear domain, the stress waveforms are often nonsinusoidal and characterized by the contribution of odd harmonics, as reported for many soft materials [37]. Hence, the nonlinear G' and G'' data extracted from the rheometer software correspond to a first harmonic approximation of the moduli (i.e., the higher order overtones are not distinguished from the fundamental frequency) and should therefore only be considered as apparent moduli. To describe the LAOS behaviors of the studied systems, we refer to the classification of the archetypal cases found for soft materials introduced by Hyun *et al.* [37]. For $0 \leq \phi_{PEO} \lesssim 0.14$, the nonlinear regime is marked by a *weak strain overshoot* (or type III LAOS behavior [37]), i.e., both moduli exhibit strain thinning when γ_0 exceeds the initial linear viscoelastic domain, with a G'' overshoot preceding its decrease. Such strain thinning eventually leads to a moduli crossover, from dominantly elastic ($G' > G''$) to dominantly viscous ($G' < G''$) behaviors, indicating an apparent fluidization of the system. For $0.14 \lesssim \phi_{PEO} \lesssim 0.63$, we observe simple

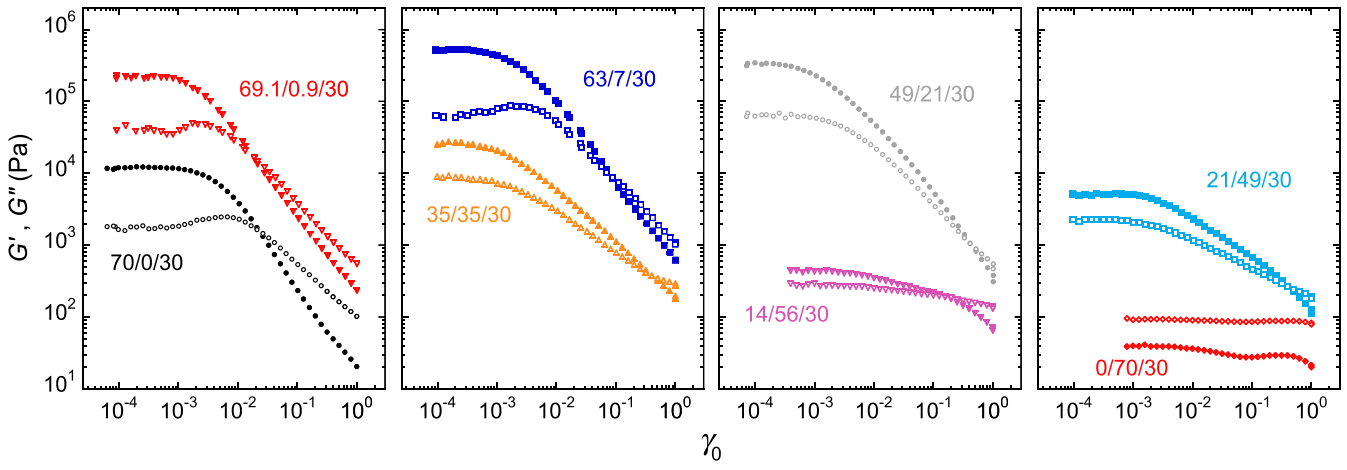

FIG. 4. Nonlinear viscoelastic response of the ternary systems during LAOS at 80 °C for $\phi = 0.30$ and $0 \leq \phi_{PEO} \leq 0.7$. The viscoelastic moduli (filled symbols, G'; open symbols, G'') correspond to the first harmonic approximation for $\omega = 1$ rad/s. Results are split in four graphs in order to enhance clarity.

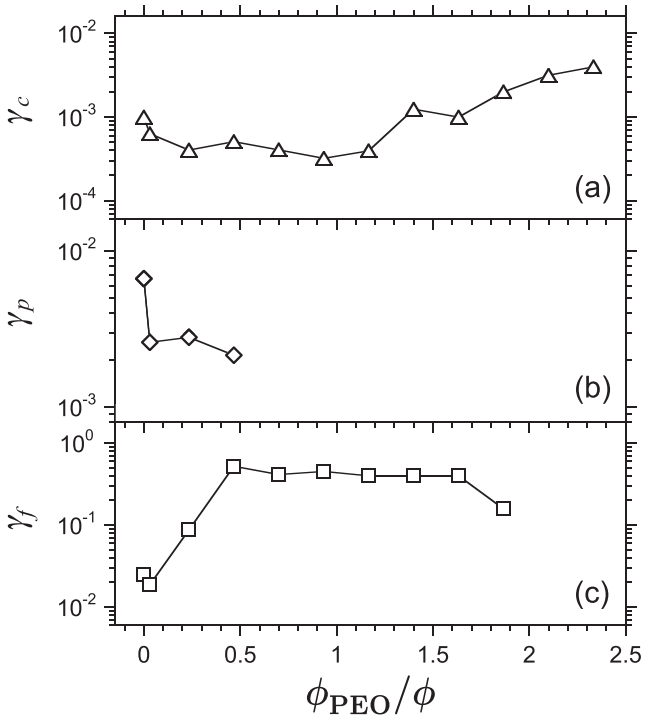

FIG. 5. Strain amplitudes measured under LAOS: (a) critical strain amplitude (limit of linearity), (b) strain amplitude at the local maximum in G'', and (c) fluidization strain amplitude vs wetting phase-to-particle volume ratio for $\phi = 0.30$.

strain thinning (or type I LAOS behavior [37]), where the monotonic decrease of both moduli with γ_0 also leads to a solidlike-to-fluidlike crossover at larger strain. Finally, a succession of *strain thinning* and *strong strain overshoot* (respectively, type I and type IV LAOS behaviors [37]) is found for $0.63 \lesssim \phi_{PEO} \leq 0.70$, with a dominantly viscous response at all strain amplitudes, an uncommon situation also encountered for soft triblock copolymer gels [38]. On a side note, the nonmonotonic evolution of the linear moduli (i.e., at small strain amplitudes) with ϕ_{PEO} is consistent with the results shown in Fig. 2.

Each set of strain sweep data shows characteristic strain amplitudes: The critical strain amplitude γ_c, which marks the onset of nonlinearity, the peak strain amplitude γ_p defined as the strain amplitude at the local maximum in loss modulus $(dG''/d\gamma_0)_{\gamma_0=\gamma_p} = 0$, and the fluidization strain amplitude γ_f, which corresponds to the strain amplitude at the apparent moduli crossover $G'(\gamma_f) = G''(\gamma_f)$. These parameters are plotted as functions of ϕ_{PEO}/ϕ in Fig. 5. For $0 \leq \phi_{PEO}/\phi \leq 0.5$, both γ_c and γ_p tend to decrease while γ_f increases significantly. Conversely, γ_c nearly plateaus before it starts increasing with the wetting phase content when $\phi_{PEO}/\phi > 0.5$. In this region, γ_p cannot be defined since the G'' overshoot disappears, and γ_f remains nearly constant. For $\phi_{PEO}/\phi \gtrsim 1.9$, the ternary systems exhibit liquidlike behavior at both small and large strain amplitudes, and hence no longer undergo to shear-induced fluidization.

Additionally, the signatures of yielding can be further investigated through parametric representations of the periodic flow parameters (aka Lissajous–Bowditch curves), i.e., stress vs strain (elastic Lissajous–Bowditch curves) and stress vs strain rate (viscous Lissajous–Bowditch curves). In the case of linear viscoelasticity, such curves display elliptic shapes, whereas nonlinear phenomena such as yielding usually translate into an anharmonic stress response, inducing more complex Lissajous–Bowditch patterns (see Supplementary Material).

D. Yielding under continuous shear

In order to further investigate the yielding transition in these ternary systems, we performed stress ramp experiments to trigger continuous shear flows. The shear viscosity and strain of the ternary systems at various compositions during the stress ramps are plotted against the shear stress in Fig. 6. For all samples, a high apparent Newtonian viscosity is observed at low stresses, followed by a significant viscosity drop as the stress increases. While the apparent low-stress Newtonian viscosity strongly depends on the ternary composition, all samples seem to converge toward $\eta \approx 20$ Pa s at high σ values regardless of their composition. Remarkably, the viscosity diminishes by a factor as high as 10^6 during the stress ramp, indicating a transition from solidlike to liquidlike behavior due to shear-induced yielding of the microstructure. The same transition can be identified in the

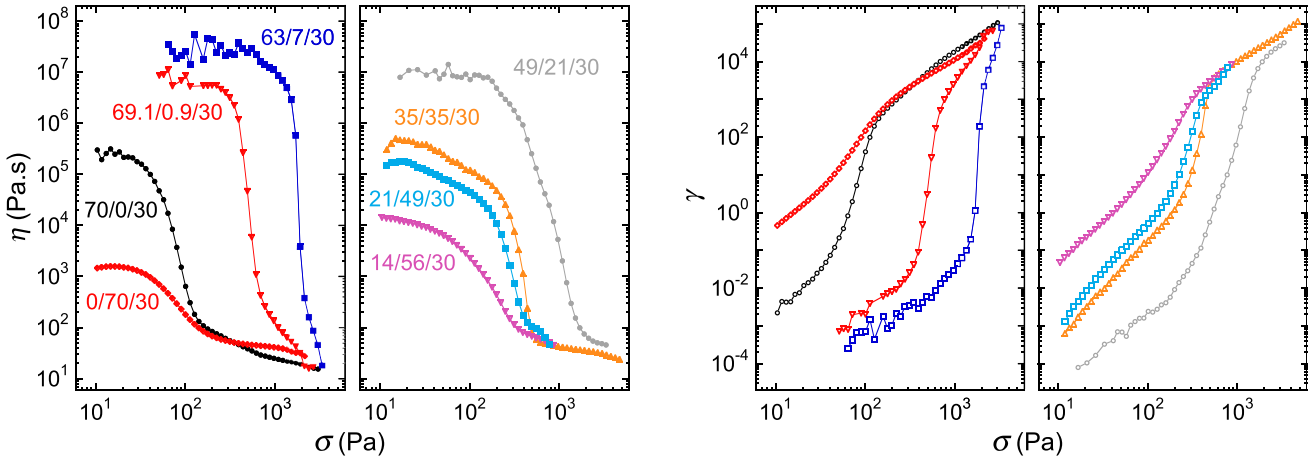

FIG. 6. Nonlinear viscoelastic response of the ternary systems during stress ramps at 80 °C for $\phi = 0.30$ and $0 \leq \phi_{PEO} \leq 0.7$: viscosity (left group) and strain (right group) vs stress.

stress–strain curves in the lower plots in Fig. 6, where a sharp rise in strain is observed. Such a transition, which occurs in a more or less narrow stress range depending on the material, is a hallmark of yield stress fluids. Its onset is likely linked to the breakage of weaker bonds within the network structure, which leads to a local viscous flow. This process progressively extends to stronger bonds as the stress increases, until the network eventually becomes fragmented, resulting in a macroscopic viscous flow. Hence, the stress range associated with the yielding transition reflects the uniformity of bond strength within the network [39], where a progressive breakdown takes place over a wide stress range (*ductile failure*), as opposed to an abrupt fragmentation process, which occurs in a narrow stress range (*brittle failure*). Here, typical brittle failure is only observed for $0 < \phi_{PEO} \lesssim 0.14$, i.e., for ternary systems in the pendular–funicular regimes, where the network modulus is maximum. Conversely, ductile failure is found for $0.14 < \phi_{PEO} \lesssim 0.56$, indicating a softer yielding transition in these systems.

As a side note, we underline that the low-stress apparent Newtonian flow regime appears in contradiction with the description of a yield stress fluid, which should behave like a solid and not like a highly viscous fluid below the yield stress. However, it is solely due to the relatively short time of these stress ramp tests, where only transient viscosity values can be captured at low stresses, as thoroughly demonstrated by Møller *et al.* [40]. In reality, the viscosity increases continuously in time when the imposed stress remains below the yield stress (see Supplementary Material).

The apparent low-stress viscosity plateau η_0, along with the strain γ_y and stress σ_y, at the yield point is plotted versus ϕ_{PEO}/ϕ in Fig. 7. As the wetting phase volume fraction increases, the yield strain γ_y tends to increase by more than two decades. On the other hand, η_0 varies similarly to G_p' [see Figs. 3(b) and 7(b)]. Finally, the yield stress σ_y marks a strong increase for $0 \leq \phi_{PEO}/\phi \lesssim 0.2$ and plateaus for $0.2 \lesssim \phi_{PEO}/\phi \lesssim 0.5$, eventually decreasing when $\phi_{PEO}/\phi \gtrsim 0.5$, which is also reminiscent of the evolution of G_p'. We note that these results are consistent with our previous study, where a similar trend was found for the evolution of σ_y over $0 \leq \phi_{PEO}/\phi < 1$, albeit at lower particle volume fraction [22].

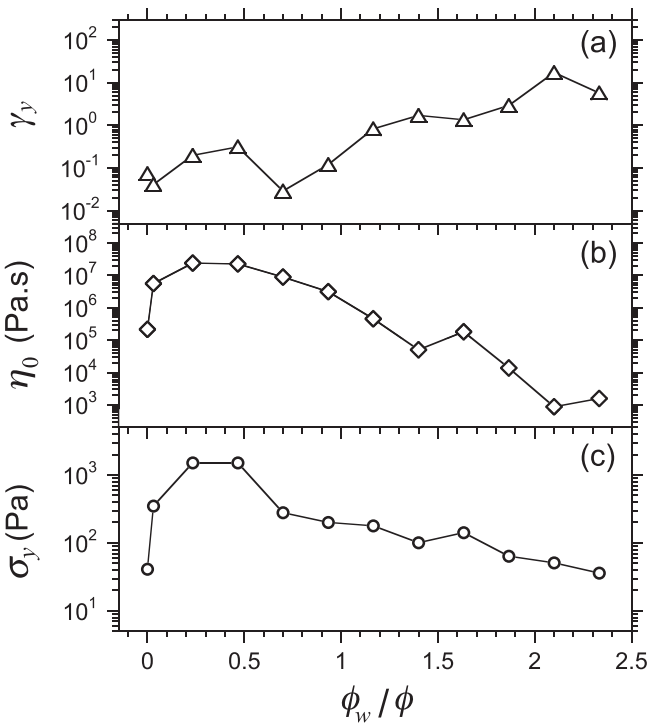

FIG. 7. (a) Yield strain, (b) zero shear viscosity, and (c) yield stress measured during stress ramps vs wetting phase-to-particle volume ratio for $\phi = 0.30$.

E. Phase inversion

Figure 1 showed that as PEO loading was increased at fixed particle content ($\phi = 0.30$), phase inversion happened: up to ~ 21 vol. % PEO, the samples had only PIB as the continuous phase, whereas samples with PEO loading at or above 42 vol. %, PEO was the dispersed phase. For intermediate PEO loadings, the samples became bicontinuous. Here, we will examine the effect of particles on phase inversion in greater detail.

Experiments similar to Fig. 1 were conducted at various particle loadings. At each particle fraction, ternary samples were prepared across a range of PEO volume fraction ϕ_{PEO}, and their morphology examined by SEM. Samples that disintegrated and dispersed in octane must have PIB as a continuous phase, whereas those that did not must have PEO as a continuous phase. A further qualitative judgement on bicontinuity was made from SEM of the cryo-fractured samples; samples with a highly tortuous interface shape were judged as being bicontinuous. We acknowledge that this is not a strict definition of bicontinuity [41], yet, since PIB is liquid at room temperature, it is not possible to extract each of the two polymers to rigorously verify bicontinuity. Figure 8 shows examples of morphologies on each side of phase inversion (the left column corresponds to the PIB-continuous samples and the right column corresponds to the PEO-continuous samples) at three particle loadings: $\phi = 0$, 0.10, and 0.20. Similar images for $\phi = 0.3$ can be found in Fig. 1. We will first discuss the morphology near phase inversion, and then the composition for phase inversion.

For particle-free blends (i.e., $\phi = 0$), a PEO-in-PIB emulsion morphology is evident for $\phi_{PEO} = 0.60$ [Fig. 8(a)], which inverts into a PIB-in-PEO emulsion morphology for $\phi_{PEO} = 0.65$ [Fig. 8(b)]. On both sides of phase inversion, drop shapes are roughly spherical, albeit with very different sizes: PIB drops in PEO are about 10 μm in diameter (with a few larger inclusions close to 100 μm in diameter). In contrast, PEO drops in PIB are much larger, typically 50 μm in diameter. This larger size of the PEO drops [Fig. 8(b) vs 8(a)] may be due to the small viscosity mismatch ($\eta_{PEO}/\eta_{PIB} \approx 1.6$ at 80 °C). Such a viscosity mismatch can influence drop breakup [42,43] and the average drop size is known to increase with increasing dispersed-to-continuous phase viscosity ratio. No bicontinuous structure could be obtained for this PIB/PEO blend system, indicating that its bicontinuity interval—if any—is likely to be very narrow.

When $\phi = 0.10$, the morphology on the PIB-rich side of phase inversion is a combination of particle-filled PEO drops and elongated PEO inclusions [Fig. 8(c)], which do not form

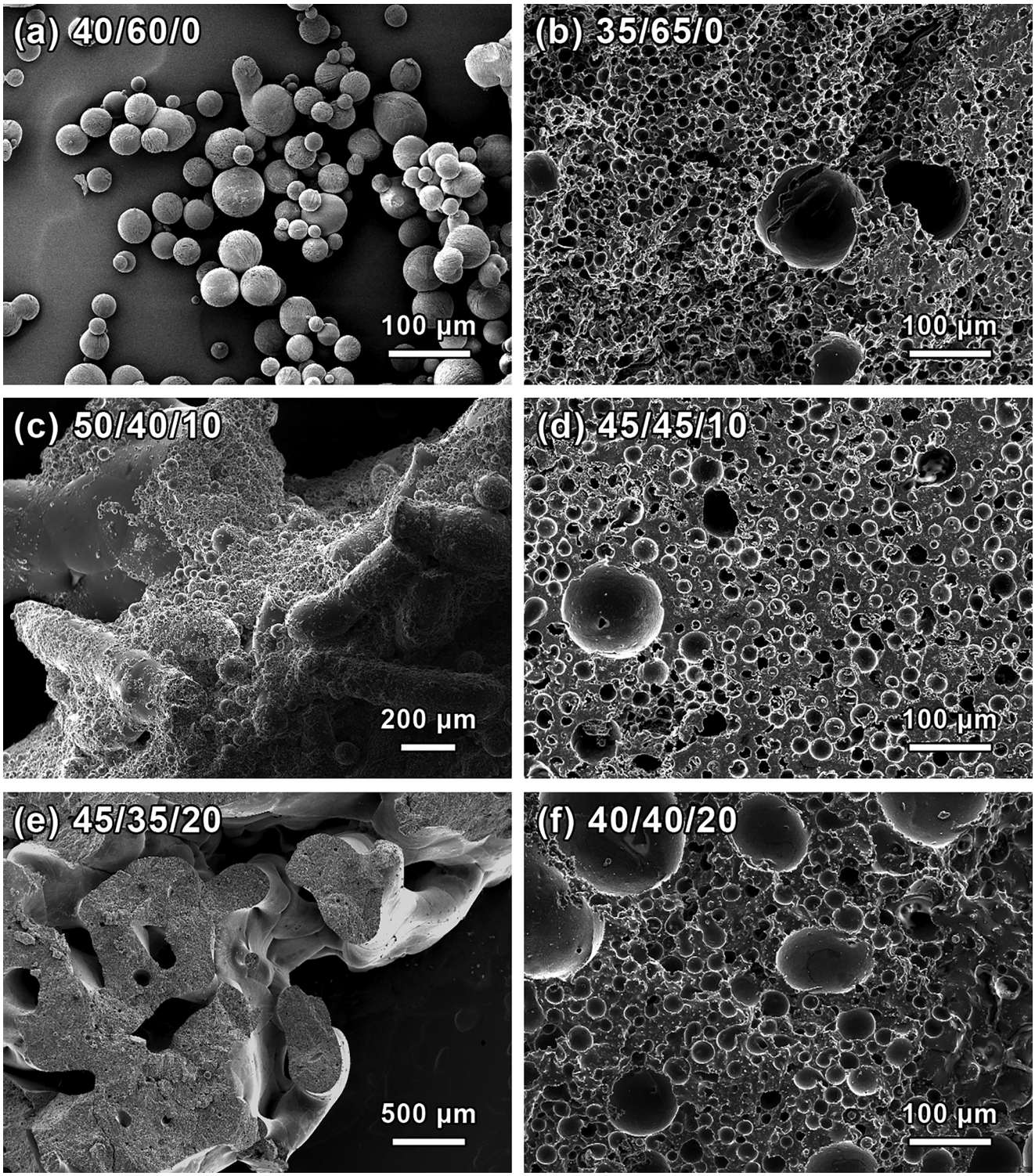

FIG. 8. SEM pictures of PIB/PEO binary systems [(a) and (b)] and PIB/PEO/SP ternary systems for $\phi = 0.10$ [(c) and (d)] and $\phi = 0.20$ [(e) and (f)] after selective dissolution of the PIB phase. All compositions are selected to straddle phase inversion.

a volume-spanning structure. Upon increasing particle loading to $\phi = 0.20$ [Fig. 8(e)], and then to $\phi = 0.30$ [Figs. 1(d) and 1(e)], there is a large increase in the size-scale of the morphology, and the interface shape becomes increasingly tortuous as the sample becomes bicontinuous. The situation is very different on the PEO-rich side of phase inversion. In the absence of particles, the PIB dispersed phase is composed of mostly 10–20 μm drops with a few much larger ($\sim$100 μm) drops. Up to a particle loading of $\phi = 0.20$, the morphology hardly changes, except perhaps an increase in the number of larger drops. At $\phi = 0.30$ [Fig. 1(f)], the dispersed phase PIB inclusions look distinctly nonspherical, with an increase in the size-scale to well over 100 μm. Thus, we qualitatively conclude that (1) the particles increase the lengthscale of the two-phase structure, (2) induce nonspherical interfacial shapes and bicontinuity at high particle

loading, and (3) have a greater effect on the morphology when the nonwetting phase is continuous.

We now turn to a more quantitative discussion of the composition at which phase inversion happens. The data of phase continuity are summarized in the ternary diagram of Fig. 9. For particle-free blends ($\phi = 0$), Figs. 8(a) and 8(b) indicate a phase inversion PEO volume fraction $\phi^{pi}_{\mathrm{PEO}} \approx 0.625 \pm 0.025$. For blends of two immiscible polymers, the phase inversion composition can be estimated based on their viscosity ratio following $\phi^{pi}_1/\phi^{pi}_2 \approx \eta_1/\eta_2$ [Pötschke and Paul (2003)] with $\phi^{pi}_1 + \phi^{pi}_2 = 1$. Qualitatively, this criterion suggests that the higher viscosity phase tends to become the dispersed phase. Here, we have $\eta_{\mathrm{PEO}}/\eta_{\mathrm{PIB}} \approx 1.6$ (measured at 80 °C) and thus $\phi^{pi}_{\mathrm{PEO}} \approx 0.615$ is expected at phase inversion, which is in excellent agreement with the experimental results.

What is striking from Fig. 9 is that the effect of particles on phase inversion is not monotonic. At low loadings, particles shift the phase inversion "leftward" i.e., toward lower ϕ_{PEO} values. Since the particles and PEO form a combined phase, we may consider the following simple idea to explain this: as a first approximation, the phase inversion occurs when the combined phase has a volume fraction $\phi + \phi_{\mathrm{PEO}} = 0.625$. This trajectory shown by the dashed blue line in Fig. 9 does show a "leftward" shift in phase inversion, but it greatly underpredicts the magnitude of the shift. We believe that the actual reason for the large shift in phase inversion composition is the interfacial activity of particles. Specifically, we have noted previously that interfacially active particles can greatly increase the drop size in droplet-matrix blends, especially if the particles are preferentially wetted by the dispersed phase system [8,44]. This suggests that particles increase the coalescence rate of the wetting phase, possibly by the bridging-dewetting mechanism known in the antifoaming literature [45]. The emulsion literature suggests that increased coalescence is a precursor to phase inversion [46], i.e., if particles accelerate coalescence of the wetting phase, then—as a consequence—continuity of the wetting phase will be favored.

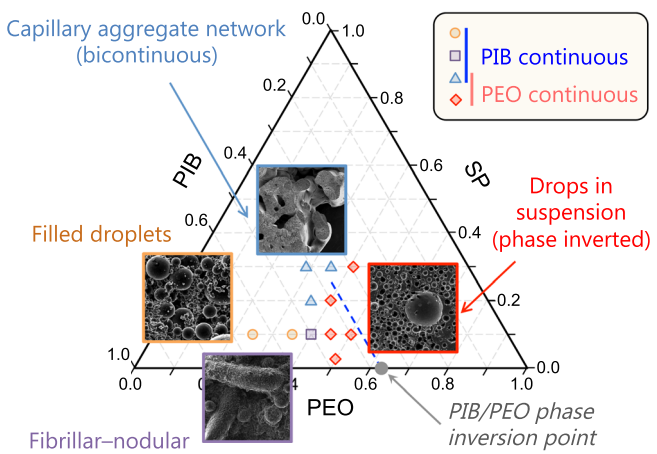

FIG. 9. Representation of the ternary composition sweeps performed to track phase inversion. The ternary composition diagram is based on volume fractions. The gray arrow at the bottom points to the estimated phase inversion point for the PIB/PEO binary system.

Throughout this article, we have regarded the particles as being fully wetted by the PEO, because the SEM images show that they can be engulfed by PEO to form a combined phase. Nevertheless, it is possible that their contact angle at the PEO/PIB interface (as measured through the PEO phase) is small but not zero, and therefore, the particles may indeed promote coalescence, e.g., by bridging-dewetting. To directly test the hypothesis that particles are interfacially active and promote coalescence, we examined one blend with a composition of PIB/PEO/SP of 47/50/3 by volume. This sample had PEO as the continuous phase, and Fig. 9 indicates a large shift in phase inversion composition as compared to $\phi = 0$. The particle loading of $\phi = 0.03$ is sufficiently dilute that the particle contribution to the bulk volume or rheology of the PEO phase may be presumed to be negligible. Thus, this result strongly supports the idea that it is the interfacial activity of particles that moves the phase inversion composition to lower wetting fluid fraction.

At higher particle loading ($\phi \gtrsim 0.24$), however, the phase inversion composition moves "rightward," and the wetting fluid fraction needed for phase inversion increases. We believe that this is attributable to rheological effects: at high particle loadings, the combined phase is a highly concentrated suspension of particles in PEO. For instance, for Fig. 1(f), which is on the PEO-rich side of phase inversion, the overall composition is PIB/PEO/SP = 28/42/30 vol. %. This corresponds to a combined phase that has 41.7 vol. % particles suspended in PEO. Thus, this combined phase may be expected to be highly viscous (in fact, Fig. 10 shows that it is solidlike in the linear viscoelastic regime). As per the simple phase inversion criterion listed above [47], this highly viscous combined phase tends to remain the dispersed phase even when the combined volume fraction $\phi + \phi_{\mathrm{PEO}}$ becomes large.

In summary, the nonmonotonic nature of the phase inversion line appears to result from two conflicting phenomena: Particle-induced coalescence tends to make the particle-wetting phase continuous, whereas the rheological consequences of adding particles tend to make the particle-wetting phase dispersed.

A final interesting issue on phase inversion is how particle migration may affect the morphology [16,48,49]. As mentioned in Sec. II A, the samples were prepared by first blending PEO and PIB, and then adding particles. Presumably, the particles first encounter the continuous phase of this PEO/PIB blend. For samples that are PIB-continuous, the particles must therefore cross the interface and migrate into the PEO phase, which indeed they do in all samples. The most interesting situation appears when the PEO:PIB ratio is near 50:50. Figure 9 then suggests that the blend is PIB-continuous prior to particle addition, but inverts after particles are added. We presume that both the particle migration as well as the phase inversion must require some mixing time, i.e., if the mixing time is much shorter, the morphology and even the phase continuity may be different from that indicated in Fig. 9.

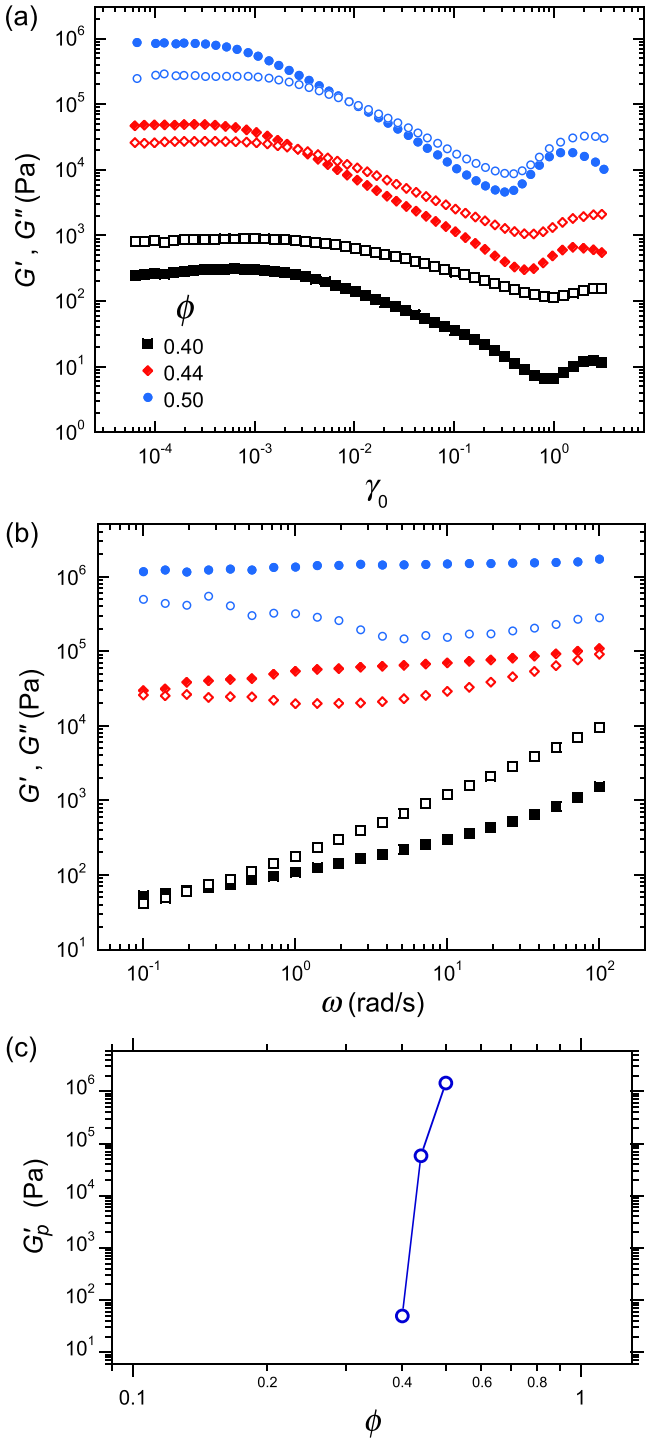

FIG. 10. Rheological behavior of concentrated PEO/SP suspensions at 80 °C: (a) apparent moduli in LAOS for $\omega = 10\,\mathrm{rad\,s^{-1}}$; (b) linear viscoelastic spectra. Filled symbols, G'; open symbols, G''. (c) Scaling of the elastic plateau modulus with particle volume fraction.

IV. DISCUSSION

A. Role of capillary cohesion in the rheological response

One of the main characteristics of the investigated ternary system is interparticle cohesion through attractive capillary forces associated with the wetting phase. Our results evidence a wide breadth of linear viscoelastic spectra, from liquidlike to solidlike behavior depending on the wetting phase content, along with pronounced fluidization phenomena under shear flow. These results will be summarized and discussed in this section. To proceed, we will make the distinction between the several microstructural regimes that characterize the considered ternary system.

First, in the pendular regime, a strong percolation network is formed through the creation of capillary bridges between the particles. This regime, which was discussed in much greater detail in our previous publication [22], corresponds to low ϕ_{PEO}/ϕ ratios. Within this regime, significant rheological changes appear even with small variations in composition. The increase in ϕ_{PEO}/ϕ allows binding more particles and pendular aggregates within the pendular network, giving rise to a stronger network with increased G_p' and σ_y and also resulting in the shortening of the linear viscoelastic domain. Such network strengthening effect results from the attractive capillary force at the particle scale, which is typically two orders of magnitude higher than the van der Waals force driving interparticle flocculation in conventional suspensions [18]. Both G_p' and σ_y continue to increase until reaching a plateau for $0.2 \lesssim \phi_{PEO}/\phi \lesssim 0.5$, where a growing fraction of the meniscus-shaped capillary bridges coalesce due to the excess of wetting phase required to connect all of the particles, which characterizes the funicular regime. Afterward, for $\phi_{PEO}/\phi \gtrsim 0.5$, G_p' and σ_y, mark a consistent decrease. The onset of this drop in elasticity and yield stress is concomitant with a structural transition from a particle network to a hierarchical network resulting from the arrested coalescence of capillary aggregates. This regime is also marked by the disappearance of the G'' overshoot during LAOS.

Up to this level of wetting phase content, the dependence of interparticle cohesion and macroscopic properties on the binding liquid volume for the investigated system reveals some parallels with the situation of wet granular media, even though in those cases the particle fraction is far higher than studied here. In particular, wet granular materials exhibit maximum strength at relatively low wetting liquid volume fractions, as assessed by tensile strength [50] and shear modulus [51] measurements. Similar to our case, this maximum occurs in a compositional region where the strength varies only slightly with the wetting phase content. The sharp increase in the strength at low wetting liquid volumes is attributed to the capillary force at the scale of particles asperities/rough regions [50,52], while the decrease in the strength with further increase in the wetting liquid volume is associated with significant coalescence of the capillary bridges [50,51]. In these studies, the maximum strength corresponds to a wetting liquid-to-particle volume ratio in the 0.03–0.08 range, which is significantly lower than the value of roughly 0.2 found in our case. We underline that, even at low wetting phase content, a purely pendular system (i.e., strictly pairwise menisci) might not be realistic in our case since the uneven drop size distribution of the PEO-in-PIB preemulsion can cause local particle aggregation in the network as well as coalescence of neighboring menisci during the mixing with particles. Instead, the investigated ternary system is more likely to evolve from a predominantly pendular configuration toward an increasingly funicular network as the wetting phase content is increased in the plateau region

(i.e., for $0.2 \lesssim \phi_{PEO}/\phi \lesssim 0.5$, where the rheology remains nearly unchanged).

Thereafter, the capillary aggregates network regime is associated with a steady decline in elasticity of the ternary system when ϕ_{PEO}/ϕ increases, during which the typical size of the primary capillary aggregates grows. We identify two reasons for this rheological trend. First, capillary aggregation implies a sharp decrease in the number of network connections as compared to a pendular network. The second is the change in internal particle packing fraction of the aggregates $\phi_{combined} = \phi/(\phi + \phi_{PEO})$. Capillary aggregates networks are typically obtained for ϕ_{PEO}/ϕ spanning from ~0.5 to ~1.2–1.8 depending on ϕ. In this range, the increase in wetting phase content causes $\phi_{combined}$ to decrease from 0.67 to 0.38–0.45.

In order to capture how the bulk rheology of the capillary aggregates is affected by this decrease in internal packing fraction, we show the results of strain sweeps and frequency sweeps performed on concentrated SP-in-PEO suspensions in Fig. 10. Strain sweeps reveal a shortening of the linear viscoelastic domain as the particle concentration increases, as well as strain thickening marked by a maximum in both apparent moduli at larger strain amplitudes [see Fig. 10(a)], in agreement with the previous results on concentrated suspensions [53]. The linear viscoelastic spectra show a transition from a liquidlike behavior at high frequencies to a weakly pronounced solidlike behavior at low frequencies for $\phi = 0.40$ [see Fig. 10(b); note that in this paragraph, ϕ refers to the particle volume fraction in the binary SP-in-PEO suspensions]. On the other hand, a solidlike behavior is found over the whole ω-range for samples with $\phi = 0.44$ and $\phi = 0.50$. As shown in Fig. 10(c), the elastic plateau modulus G'_p grows sharply with ϕ for $0.40 \leq \phi \leq 0.50$ indicating that the sample becomes strongly solidlike around $\phi = 0.45$.

Consequently in the ternary system, an increase in ϕ_{PEO}/ϕ results in a significant decrease in bulk elasticity of the capillary aggregates, which lowers the modulus of the capillary aggregate network and leads to a higher degree of partial coalescence between the aggregates. Moreover, the increase in the wetting phase content leads to the formation of capillary aggregates with larger size and less concentrated in particles, and ultimately causes the PEO–PIB interface to become smoother. This lowering of the interfacial curvature reduces the Laplace pressure acting on the particles and hence the cohesion of the aggregates. In these conditions, merging of the particle-filled PEO domain is favored and the ternary system undergoes phase inversion, i.e., the PEO becomes the sole continuous phase while the PIB phase forms drops. The rheological response is found to be slightly nonmonotonic around the phase inversion composition, where both G'_p and σ_y show a shallow secondary increase for ϕ_{PEO}/ϕ between 1.1 and 1.9 [see Figs. 3(b) and 8(c)]. The reason for such trend is not clear but could be linked to the strongly heterogeneous nature of the microstructure close to phase inversion.

Following phase inversion, the morphology becomes that of drops-in-suspension, where the particles remained solely located in the continuous PEO phase. Near phase inversion, many PIB drops, especially large ones, have not relaxed to a spherical shape [see Fig. 1(f)]. Since the PIB drops are located within a concentrated SP-in-PEO suspension [the particle concentration in the PEO phase is given by $\phi_{combined} = \phi/(\phi + \phi_{PEO}) \approx 0.42$ for the composition corresponding to Fig. 1(f)], their nonspherical shape is likely due to the long relaxation time associated with the solidlike viscoelasticity of the continuous phase, given that the morphology of the ternary system is frozen rapidly after completion of the mixing process. In this regime, increasing ϕ_{PEO} at fixed ϕ dilutes the particles in the continuous phase PEO (i.e., $\phi_{combined}$ reduces). Hence, it leads to a decrease of the viscoelastic moduli of the continuous phase, which fosters the full relaxation of PIB drops to spherical shape.

B. Ternary morphological map construction

Our results provide the basis for full morphological mapping of the investigated ternary system. The characteristic structures are summarized in a ternary diagram based on volume fractions in Fig. 11. The transitions in this map include insights from both the results of this paper and some previous results at lower particle loading. Figure 11 marks the maximum particle packing fraction to the random close packing fraction for monodisperse spheres $\phi_{RCP} \approx 0.64$ [54]. This limit is represented by the white region in the upper corner of the ternary diagram (Fig. 11), which is experimentally out of reach for nondeformable particles. We previously established the boundaries of the pendular ($0 < \phi_{PEO}/\phi \lesssim 0.22$) and funicular ($0.22 \lesssim \phi_{PEO}/\phi \lesssim 0.53$) regimes, as well as the low boundary for the capillary aggregates regime ($0.53 \lesssim \phi_{PEO}/\phi$), based on experimental data at $\phi = 0.10$ and geometric arguments [22]. Here, these transitions are confirmed at higher particle concentration (i.e., $\phi = 0.30$). Moreover, we now can determine the upper boundary for the capillary aggregates regime, which shows a more intricate dependence on ϕ.

The bicontinuous structures based on the arrested coalescence of capillary aggregates constitute a robust feature of the investigated ternary system. They are observed over a wide region of the ternary compositional space (see Fig. 11), in contrast with the particle-free PIB/PEO binary system, in which bicontinuity is restricted to a very narrow composition range (see Sec. III E) and is unstable by nature due to coarsening. On the other hand, the bicontinuous structures obtained in the case of ternary systems were very stable even when the two polymers were kept molten [29]. Such stability against fluid phases coarsening likely results from the solidlike dynamics associated with selective partitioning of the particles within the wetting phase. Indeed, similar observations were made in polymer blends, where the addition of solid fillers leads to a broadening of the composition range for bicontinuity [55–57].

At low/intermediate particle content (typically for $\phi < 0.20$), the increase in wetting phase content can destabilize the bicontinuous structures and lead to a filled drop morphology, i.e., particle-filled PEO droplets dispersed within the PIB continuous phase, prior to phase inversion of the system. Such particles-in-drops microstructures can exhibit a mixed fibrillar–nodular morphology as the composition

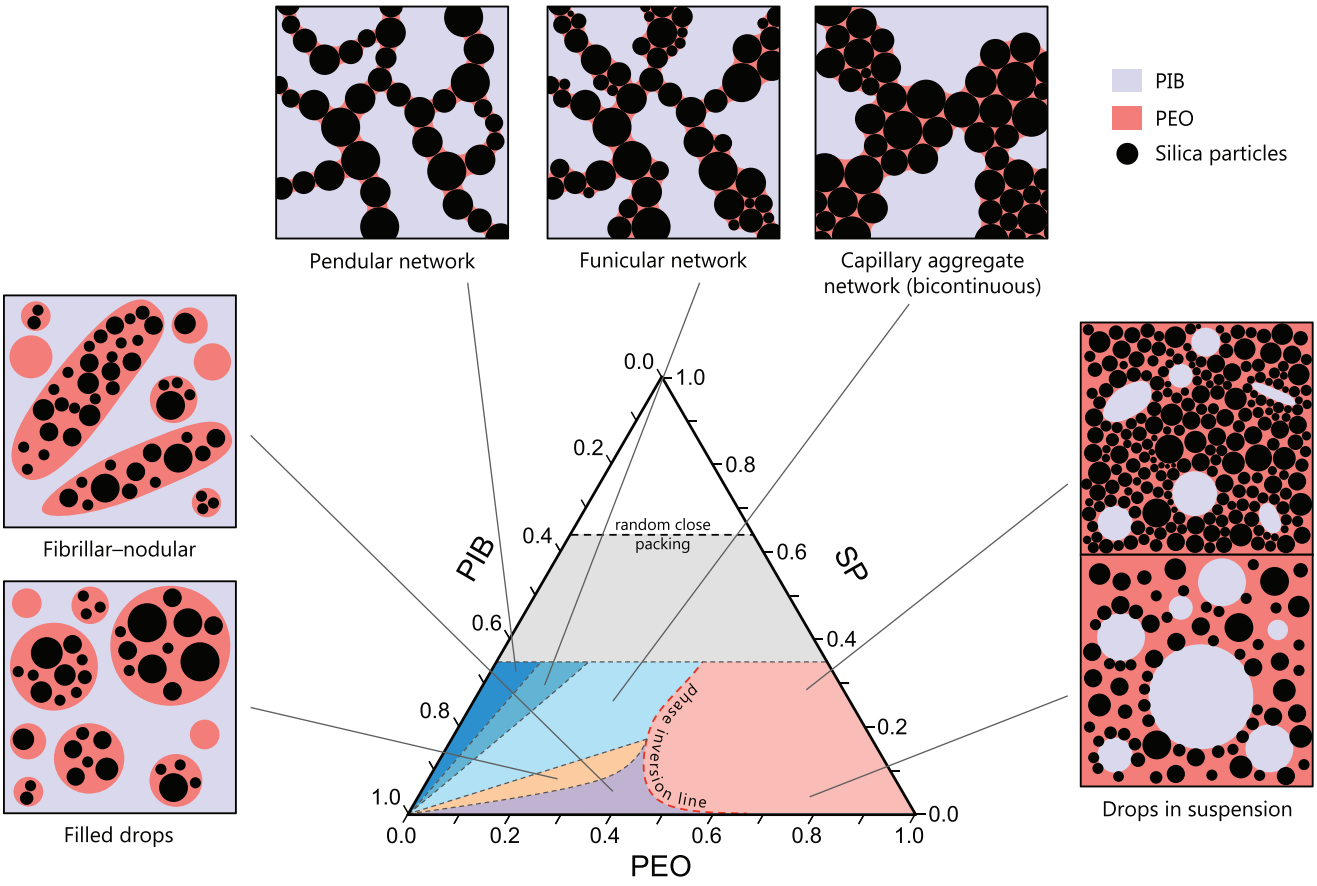

FIG. 11. Morphological mapping and schematic structures of the investigated PIB/PEO/SP ternary system. The ternary composition diagram is based on volume fractions. The red dashed path in the ternary diagram represents the phase inversion boundary, with the liquid continuous phase being PIB (nonwetting phase) on the left-hand side and PEO (wetting phase) on the right-hand side. The gray region of the ternary diagram above $\phi_p = 0.35$ corresponds to high particle concentrations, which is unexplored here. The upper limit in particle volume fraction is marked at the random close packing for monodisperse spheres $\phi_{RCP} \approx 0.64$. Note that the network structures are volume-spanning only above the percolation threshold, i.e., for $\phi > \phi_{per} \approx 0.05$.

approaches the phase inversion boundary. This may arise because some PEO inclusions have a slightly higher particle loading, thus arresting them in highly nonspherical shapes.

When approaching phase inversion from the PIB-continuous side, the ternary system is thus either a nonpercolating particles-in-drops microstructure or a selectively filled bicontinuous network, where the route to phase inversion depends on ϕ. As shown by the red dashed line in Fig. 11, the presence of particles in the wetting phase favors continuity of the latter at low ϕ, while the bicontinuous structures appear to repel the phase inversion boundary so that continuity of the nonwetting phase is favored at higher ϕ. This reveals that phase coarsening is strongly influenced by the particle concentration due to the competition between particle-induced coalescence and particle-jamming of the wetting phase. Similar dynamic coupling in ternary blends with selective localization of the solid particles in one of the fluid phases was shown by Tanaka *et al.* [58] through 2D experiments, where the particle volume fraction was found to influence the coarsening dynamics of the system.

Once phase inversion occurs, the ternary system adopts a drops-in-suspension configuration where the particles can either be engulfed by the PEO or adsorb at the PIB–PEO interface. However, due to the low affinity between particles and PIB, the particles tend to stay in the PEO phase, with minimal contact at the PIB–PEO interface. Since the particles in all samples appear overwhelmingly in the PEO phase, the contact angle θ (as defined through the PEO phase) can be assumed to be very small or near zero. Such small contact angles are insufficient to stabilize Pickering emulsions, and additional viscous forces during mixing likely further destabilize any weak Pickering emulsion that may form. Finally, when the particle content increases (moving upward in the ternary diagram), the SP-in-PEO suspension becomes solidlike, which tends to delay the relaxation of the drops and hence favors the presence of unrelaxed nonspherical drops.

V. CONCLUSIONS

In summary, we have investigated the microstructural transitions present in liquid–liquid–particle ternary systems and their influence on the rheology. Such three-phase systems encompass the components of suspensions and emulsions within a single framework, where the wetting properties of the particles toward each of the fluid phases have a significant impact on the ternary structural diagram. Our study has focused on the singular case of strong preferential wetting of the particles by one of the viscous fluid

polymer phases. We have identified, for the first time in one single system, five main classes of morphology that constitute the complete structural diagram of such ternary systems: (1) pendular network, (2) funicular network, (3) capillary aggregates network, (4) filled drops, and (5) drops-in-suspension. Our results highlight the central role of capillary interactions in the formation of percolated structures in the case of pendular, funicular, and capillary aggregates bicontinuous networks, where the cohesion between the particles forming the network is dominated by capillary forces. For a fixed particle volume fraction, the increase in wetting phase volume fraction induces a change in the building blocks of the capillary-driven network from single particles to capillary aggregates. In the latter case, the resulting material is a bicontinuous gel with a selectively particle-filled domain, which completely differs from the bijel structure obtained in the case of particles with neutral wettability. The formation of such hierarchical network leads to an extended composition interval for bicontinuity as compared to the particle-free polymer blend, in accordance with several examples from the literature dealing with polymer–polymer–colloidal particle ternary blends with strong selective partitioning of the particles in one of the polymer phases. In addition, the particle volume fraction was found to have a strong influence on phase inversion of the ternary system. While continuity of the wetting phase is promoted at low particle volume fractions, likely due to interfacial activity-induced coalescence, at higher particle volume fractions, the interplay between capillary cohesion and phase coarsening of the immiscible fluids leads to a delayed phase inversion from nonwetting phase continuity to wetting phase continuity.

From a rheological standpoint, interparticle capillary cohesion results in a manifest strengthening of the ternary system, where the elastic plateau modulus and yield stress significantly increase up to the funicular state. A microstructural switch from a capillary-driven particle network to a particle aggregate network then leads to a decrease in elasticity. The maximum in elastic plateau modulus and yield stress is observed at a wetting phase-to-particle volume ratio around 0.2–0.5, in agreement with our previous study conducted at lower particle concentration. The yielding behavior also depends on the morphology since a transition from brittle to ductile yielding is found as the phase inversion boundary from bicontinuous structure to suspension–emulsion is crossed.

This study should provide a practical basis for the design of soft materials based on the ternary liquid–liquid–solid particle that blends with selective wetting properties, and for tuning their microstructure and rheology. Other important aspects, such as the influence of particle wettability on the proposed ternary mapping, the universality of the ternary phase behavior for polymeric and small molecules liquids, as well as the influence of the size and shape of the solid particles, remain to be fully addressed.

ACKNOWLEDGMENTS

The authors thank Junyi Yang for his help with samples preparation. This work was supported by the National Science Foundation under NSF-CBET Grant Nos. 0932901 and 1336311.

References

[1] Mason, T. G., and D. A. Weitz, "Linear viscoelasticity of colloidal hard sphere suspensions near the glass transition," Phys. Rev. Lett. **75**, 2770–2773 (1995).

[2] Mason, T. G., J. Bibette, and D. A. Weitz, "Elasticity of compressed emulsions," Phys. Rev. Lett. **75**, 2051–2054 (1995).

[3] Ramsden, W., "Separation of solids in the surface-layers of solutions and 'suspensions' (observations on surface-membranes, bubbles, emulsions, and mechanical coagulation).—Preliminary account," Proc. Roy. Soc. London **72**, 156–164 (1903).

[4] Pickering, S. U., "CXCVI—Emulsions," J. Chem. Soc. **91**, 2001–2021 (1907).

[5] Binks, B. P., and T. S. Horozov, "Colloidal particles at liquid interfaces: An introduction," in *Colloidal Particles at Liquid Interfaces*, edited by B. P. Binks and T. S. Horozov (Cambridge University, Cambridge, 2006).

[6] Fenouillot, F., P. Cassagnau, and J. C. Majesté, "Uneven distribution of nanoparticles in immiscible fluids: Morphology development in polymer blends," Polymer **50**, 1333–1350 (2009).

[7] Lee, M. N., H. K. Chan, and A. Mohraz, "Characteristics of pickering emulsion gels formed by droplet bridging," Langmuir **28**, 3085–3091 (2012).

[8] Nagarkar, S. P., and S. S. Velankar, "Morphology and rheology of ternary fluid-fluid-solid systems," Soft Matter **8**, 8464–8477 (2012).

[9] Stancik, E. J., and G. G. Fuller, "Connect the drops: Using solids as adhesives for liquids," Langmuir **20**, 4805–4808 (2004).

[10] Horozov, T. S., and B. P. Binks, "Particle-stabilized emulsions: A bilayer or a bridging monolayer?," Ange. Chem. **118**, 787–790 (2006).

[11] Herzig, E. M., K. A. White, A. B. Schofield, W. C. K. Poon, and P. S. Clegg, "Bicontinuous emulsions stabilized solely by colloidal particles," Nat. Mater. **6**, 966–971 (2007).

[12] Cates, M. E., and P. S. Clegg, "Bijels: A new class of soft materials," Soft Matter **4**, 2132–2138 (2008).

[13] Cai, D., and P. S. Clegg, "Stabilizing bijels using a mixture of fumed silica nanoparticles," Chemical Communications (2015).

[14] Calberg, C., S. Blacher, F. Gubbels, F. Brouers, R. Deltour, and R. Jérôme, "Electrical and dielectric properties of carbon black filled co-continuous two-phase polymer blends," J. Phys. D: Appl. Phys. **32**, 1517–1525 (1999).

[15] Gubbels, F., R. Jerome, P. Teyssie, E. Vanlathem, R. Deltour, A. Calderone, V. Parente, and J. L. Bredas, "Selective localization of carbon black in immiscible polymer blends: A useful tool to design electrical conductive composites," Macromolecules **27**, 1972–1974 (1994).

[16] Gubbels, F., R. Jerome, E. Vanlathem, R. Deltour, S. Blacher, and F. Brouers, "Kinetic and thermodynamic control of the selective localization of carbon black at the interface of immiscible polymer blends," Chem. Mater. **10**, 1227–1235 (1998).

[17] Bai, L., J. W. Fruehwirth, X. Cheng, and C. W. Macosko, "Dynamics and rheology of nonpolar bijels," Soft Matter **11**, 5282–5293 (2015).

[18] Koos, E., and N. Willenbacher, "Capillary forces in suspension rheology," Science **331**, 897–900 (2011).

[19] Koos, E., J. Johannsmeier, L. Schwebler, and N. Willenbacher, "Tuning suspension rheology using capillary forces," Soft Matter **8**, 6620–6628 (2012).

[20] Heidlebaugh, S. J., T. Domenech, S. V. Iasella, and S. S. Velankar, "Aggregation and separation in ternary particle/oil/water systems with fully wettable particles," Langmuir **30**, 63–74 (2014).

[21] Domenech, T., and S. Velankar, "Capillary-driven percolating networks in ternary blends of immiscible polymers and silica particles," Rheol. Acta **53**, 593–605 (2014).
[22] Domenech, T., and S. S. Velankar, "On the rheology of pendular gels and morphological developments in paste-like ternary systems based on capillary attraction," Soft Matter **11**, 1500–1516 (2015).
[23] Bossler, F., and E. Koos, "Structure of particle networks in capillary suspensions with wetting and nonwetting fluids," Langmuir **32**, 1489–1501 (2016).
[24] Zhang, J., H. Zhao, W. Li, M. Xu, and H. Liu, "Multiple effects of the second fluid on suspension viscosity," Sci. Rep. **5**, 16058 (2015).
[25] Strauch, S., and S. Herminghaus, "Wet granular matter: A truly complex fluid," Soft Matter **8**, 8271–8280 (2012).
[26] Koos, E., "Capillary suspensions: Particle networks formed through the capillary force," Curr. Opin. Colloid Interface Sci. **19**, 575–584 (2014).
[27] Brunschwiler, T., G. Schlottig, S. Ni, Y. Liu, J. V. Goicochea, J. Zurcher, and H. Wolf, "Formulation of percolating thermal underfills using hierarchical self-assembly of micro- and nanoparticles by centrifugal forces and capillary bridging," Proceedings of the 45th International Symposium on Microelectronics, San Diego, California (2012).
[28] Velankar, S. S., "A non-equilibrium state diagram for liquid/fluid/particle mixtures," Soft Matter **11**, 8393–8403 (2015).
[29] Domenech, T., J. Yang, S. Heidlebaugh, and S. S. Velankar, "Three distinct open-pore morphologies from a single particle-filled polymer blend," Phys. Chem. Chem. Phys. **18**, 4310–4315 (2016).
[30] Iveson, S. M., J. A. Beathe, and N. W. Page, "The dynamic strength of partially saturated powder compacts: The effect of liquid properties," Powder Technol. **127**, 149–161 (2002).
[31] See supplementary material at http://dx.doi.org/10.1122/1.4975931 for additional SEM, discussion of Lissajous–Bowditch plots and transient regime under creep.
[32] Koumakis, N., and G. Petekidis, "Two step yielding in attractive colloids: Transition from gels to attractive glasses," Soft Matter **7**, 2456–2470 (2011).
[33] Liu, A. J., S. Ramaswamy, T. G. Mason, H. Gang, and D. A. Weitz, "Anomalous viscous loss in emulsions," Phys. Rev. Lett. **76**, 3017–3020 (1996).
[34] Hébraud, P., F. Lequeux, and J. F. Palierne, "Role of permeation in the linear viscoelastic response of concentrated emulsions," Langmuir **16**, 8296–8299 (2000).
[35] Gopal, A. D., and D. J. Durian, "Relaxing in foam," Phys. Rev. Lett. **91**, 188303 (2003).
[36] Pusey, P. N., and W. van Megen, "Observation of a glass transition in suspensions of spherical colloidal particles," Phys. Rev. Lett. **59**, 2083–2086 (1987).
[37] Hyun, K., M. Wilhelm, C. O. Klein, K. S. Cho, J. G. Nam, K. H. Ahn, S. J. Lee, R. H. Ewoldt, and G. H. McKinley, "A review of nonlinear oscillatory shear tests: Analysis and application of large amplitude oscillatory shear (LAOS)," Prog. Polym. Sci. **36**, 1697–1753 (2011).
[38] Hyun, K., J. Nam, M. Wilhellm, K. Ahn, and S. Lee, "Large amplitude oscillatory shear behavior of PEO-PPO-PEO triblock copolymer solutions," Rheol. Acta **45**, 239–249 (2006).
[39] Uhlherr, P. H. T., J. Guo, C. Tiu, X. M. Zhang, J. Z. Q. Zhou, and T. N. Fang, "The shear-induced solid–liquid transition in yield stress materials with chemically different structures," J. Non-Newtonian Fluid Mech. **125**, 101–119 (2005).
[40] Møller, P. C. F., A. Fall, and D. Bonn, "Origin of apparent viscosity in yield stress fluids below yielding," Europhys. Lett. **87**, 38004 (2009).
[41] Galloway, J. A., and C. W. Macosko, "Comparison of methods for the detection of cocontinuity in poly(ethylene oxide)/polystyrene blends," Polym. Eng. Sci. **44**, 714–727 (2004).
[42] Favis, B. D., and J. P. Chalifoux, "The effect of viscosity ratio on the morphology of polypropylene/polycarbonate blends during processing," Polym. Eng. Sci. **27**, 1591–1600 (1987).
[43] Sundararaj, U., and C. W. Macosko, "Drop breakup and coalescence in polymer blends: The effects of concentration and compatibilization," Macromolecules **28**, 2647–2657 (1995).
[44] Thareja, P., K. Moritz, and S. S. Velankar, "Interfacially active particles in droplet/matrix blends of model immiscible homopolymers: Particles can increase or decrease drop size," Rheol. Acta **49**, 285–298 (2010).
[45] Garrett, P. R., *Defoaming: Theory and Industrial Applications* (Taylor & Francis, Boca Raton, 1992).
[46] Davies, J. T., "A quantitative kinetic theory of emulsion type. I. Physical chemistry of the emulsifying agent," in *Gas/Liquid and Liquid/Liquid Interfaces* (Butterworths, London, 1957).
[47] Pötschke, P., and D. R. Paul, "Formation of co-continuous structures in melt-mixed immiscible polymer blends," J. Macromol. Sci. C **43**, 87–141 (2003).
[48] Jalali Dil, E., and B. D. Favis, "Localization of micro and nano-silica particles in a high interfacial tension poly(lactic acid)/low density polyethylene system," Polymer **77**, 156–166 (2015).
[49] Elias, L., F. Fenouillot, J. C. Majesté, G. Martin, and P. Cassagnau, "Migration of nanosilica particles in polymer blends," J. Polym. Sci. B: Polym. Phys. **46**, 1976–1983 (2008).
[50] Scheel, M., R. Seemann, M. Brinkmann, M. Di Michiel, A. Sheppard, B. Breidenbach, and S. Herminghaus, "Morphological clues to wet granular pile stability," Nat. Mater. **7**, 189–193 (2008).
[51] Møller, P. C. F., and D. Bonn, "The shear modulus of wet granular matter," Europhys. Lett. **80**, 38002 (2007).
[52] Halsey, T. C., and A. J. Levine, "How sandcastles fall," Phys. Rev. Lett. **80**, 3141–3144 (1998).
[53] Heymann, L., S. Peukert, and N. Aksel, "Investigation of the solid–liquid transition of highly concentrated suspensions in oscillatory amplitude sweeps," J. Rheol. **46**, 93–112 (2002).
[54] Scott, G. D., "Packing of spheres: Packing of equal spheres," Nature **188**, 908–909 (1960).
[55] Steinmann, S., W. Gronski, and C. Friedrich, "Influence of selective filling on rheological properties and phase inversion of two-phase polymer blends," Polymer **43**, 4467–4477 (2002).
[56] Wu, G., B. Li, and J. Jiang, "Carbon black self-networking induced co-continuity of immiscible polymer blends," Polymer **51**, 2077–2083 (2010).
[57] Zhang, M., Y. Huang, M. Kong, H. Zhu, G. Chen, and Q. Yang, "Morphology and rheology of poly(l-lactide)/polystyrene blends filled with silica nanoparticles," J. Mater. Sci. **47**, 1339–1347 (2012).
[58] Tanaka, H., A. J. Lovinger, and D. D. Davis, "Pattern evolution caused by dynamic coupling between wetting and phase separation in binary liquid mixture containing glass particles," Phys. Rev. Lett. **72**, 2581–2584 (1994).